Requirement of translocated lysosomal V1 H^+-ATPase for activation of membrane acid sphingomyelinase and raft clustering in coronary endothelial cells

Ming Xu, Min Xia, Xiao-Xue Li, Wei-Qing Han, Krishna M. Boini, Fan Zhang, Yang Zhang, Joseph K Ritter, and Pin-Lan Li

Department of Pharmacology and Toxicology, Medical College of Virginia, Virginia Commonwealth University, Richmond, VA 23298

ABSTRACT **Acid sphingomyelinase (ASM) mediates the formation of membrane raft (MR) redox signalosomes in a process that depends on a local acid microenvironment in coronary arterial endothelial cells (CAECs). However, it is not known how this local acid microenvironment is formed and maintained. The present study hypothesized that lysosomal V1 H^+-ATPase provides a hospitable acid microenvironment for activation of ASM when lysosomes traffic and fuse into the cell membrane. Confocal microscopy showed that local pH change significantly affected MRs, with more fluorescent patches under low pH. Correspondingly, the ASM product, ceramide, increased locally in the cell membrane. Electron spin resonance assay showed that local pH increase significantly inhibited NADPH oxidase–mediated production of $O_2^{-\cdot}$ in CAECs. Direct confocal microscopy demonstrated that Fas ligand resulted in localized areas of decreased pH around CAEC membranes. The inhibitors of both lysosomal fusion and H^+-ATPase apparently attenuated FasL-caused pH decrease. V1 H^+-ATPase accumulation and activity on cell membranes were substantially suppressed by the inhibitors of lysosomal fusion or H^+-ATPase. These results provide the first direct evidence that translocated lysosomal V1 H^+-ATPase critically contributes to the formation of local acid microenvironment to facilitate activation of ASM and consequent MR aggregation, forming MR redox signalosomes and mediating redox signaling in CAECs.**

Monitoring Editor
Jean E. Gruenberg
University of Geneva

Received: Sep 28, 2011
Revised: Feb 6, 2012
Accepted: Feb 14, 12

This article was published online ahead of print in MBoC in Press (http://www.molbiolcell.org/cgi/doi/10.1091/mbc.E11-09-0821) on February 22, 2012.

Address correspondence to: Pin-Lan Li (pli@vcu.edu).

Abbreviations used: Ami, amitriptyline; ASM, acid sphingomyelinase; Baf, bafilomycin A1; CAECs, coronary arterial endothelial cells; CMH, 1-hydroxy-3-methoxycarbonyl-2,2,5,5-tetramethylpyrrolidine; CtxB, cholera-toxin B; DHE, dihydroethidine; ESR, eletromagnetic spin resonance; FasL, Fas ligand; FRET, fluorescence resonance energy transfer; Lamp-1, lysosomal-associated membrane protein 1; LC–ESI–MS, liquid chromatography–electrospray ionization–tandem mass spectrometry; MCD, methyl-β-cyclodextrin; MRs, membrane rafts; $O_2^{-\cdot}$, superoxide; OG488, Oregon Green 488 carboxylic acid, succinimidyl ester; ROS, reactive oxygen species; SNARE, soluble *N*-ethylmaleimide-sensitive factor attachment protein receptor; TRITC, tetramethylrhodamine isothiocyanate; TT, tetanus toxin; Vamp-2, vesicle-associated membrane proteins 2.

INTRODUCTION

Lipid rafts (LRs), which consist of dynamic assemblies of cholesterol and lipids with saturated acyl chains in the membrane of cells (Bollinger *et al*., 2005), play an essential role in signal transduction (Cherukuri *et al*., 2001; Brown, 2006; Allen *et al*., 2007; Yamazaki *et al*., 2007). Because many studies indicated that raft formation is not driven solely by lipids but also by protein interactions (Pike, 2006), it is more appropriate that these rafts are referred to as membrane rafts (MRs; Zhang and Li, 2010). The clustered MRs can recruit or aggregate various signaling molecules to form platforms that initiate receptor-mediated transmembrane signal transduction in a variety of mammalian cells (Gupta and DeFranco, 2003; Li *et al*., 2007; Yamazaki *et al*., 2007; Kuebler *et al*., 2010; Li *et al*., 2010). For example, we demonstrated that MR clustering on the arterial endothelium could recruit some redox signaling molecules, including NADPH oxidase subunits and Rac GTPase, to impair endothelial

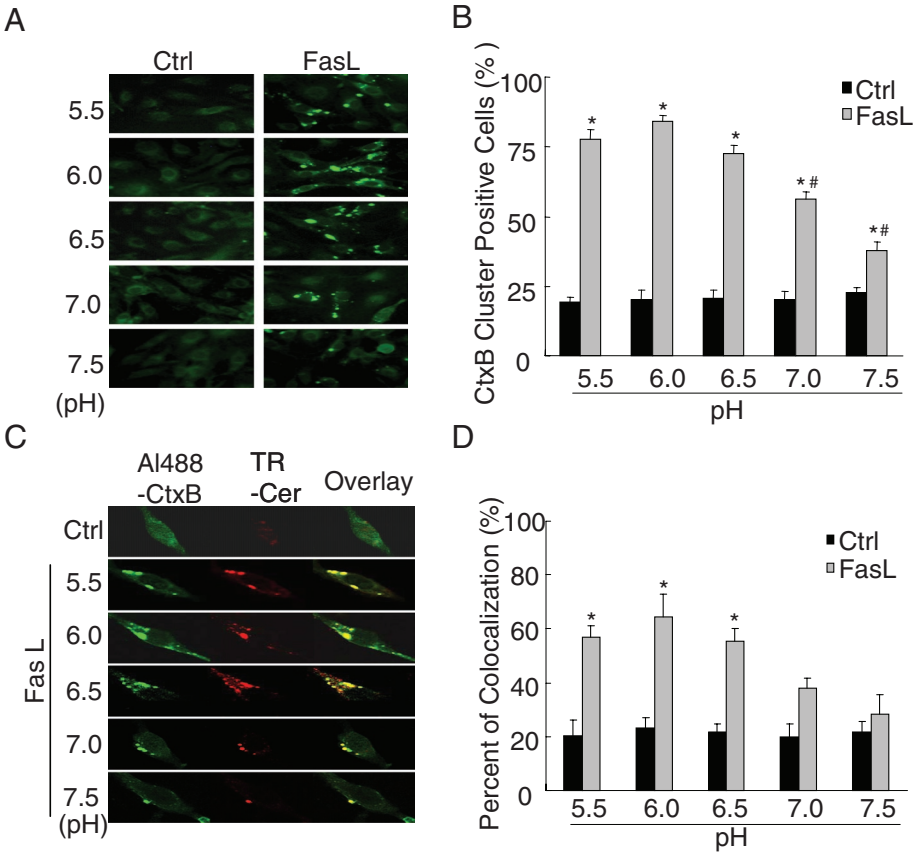

FIGURE 1: Effects of pH change on the colocalization of CtxB-staining fluorescent patches and ceramide. (A) Representative confocal microscopic images of CAECs stained by Al488-CtxB. (B) Summary of effects showing that FasL significantly increased the percentage of CtxB cluster–positive cells stained by Al488-CtxB at pH 5.5, 6.0, 6.5, 7.0, and 7.5. (C) Representative confocal microscopic images of the colocalization of CtxB-staining patches and ceramide in FasL-treated CAECs at different pH. Al488-CtxB is shown as a pseudo green on the left; Texas red–conjugated anti-ceramide is shown as red in the middle; and overlaid images are shown on the right. Yellow spots in the overlaid images were defined as patches of the colocalization in CtxB-staining patches and ceramide. The images are representatives from six separate batches of CAECs. (D) Percentage changes in positive cells costained by Al488-CtxB and anticeramide antibody during FasL stimulation ($n = 6$, $^{*}p < 0.05$ vs. control; $^{\#}p < 0.05$ vs. pH = 6.0 group).

function by enhanced production of reactive oxygen species (ROS; Zhang *et al.*, 2006).

Our recent studies indicated that MR redox signaling in coronary arterial endothelial cells (CAECs) is related to the increased activity of lysosomal acid sphingomyelinase (ASM), which hydrolyzes membrane-bound sphingomyelin into the bioactive lipid ceramide (Zhang *et al.*, 2007). Lysosome-associated vesicle transportation or trafficking of ASM from the abluminal compartment to the cell membrane is a prerequisite for ASM activation (Jin *et al.*, 2008a). In addition, ASM is characterized by working optimally at acidic pH (Schuchman, 2010). Thus it is expected that an acid microenvironment around the cell membrane is critical to the formation of MR redox signaling by ASM activation. However, the mechanism by which the acid environment is formed remains obscure.

It is generally accepted that some factors, including proton leak, ClC chloride channels, or Na^+/K^+-ATPase, participate in the regulation of extracellular or intracellular pH. Among these factors, the activity of the vacuolar H^+-ATPase is regarded as a primary factor of pH regulation (Zou *et al.*, 2010). H^+-ATPase is a multisubunit transmembrane complex responsible for pumping protons from the cytoplasm to the lumen of organelles or outside the cell (Forgac, 2007). As a consequence, H^+-ATPase plays a role in acidifying the extracellular medium or controlling the cytoplasmic pH (Li *et al.*, 1999). On the lysosomal membrane, H^+-ATPase functions to acidify the vesicle compartmental environment, thereby facilitating the activities of various acid hydrolases. When endothelial cells (ECs) are stimulated by death-receptor agonists such as Fas ligand (FasL) or tumor necrosis factor α, lysosomal vesicles traffic or migrate to the cell membrane (Bao *et al.*, 2010b). It was reported that phagosome acidification occurs by direct recruitment of H^+-ATPase derived from lysosomes (Sun-Wada *et al.*, 2009), which provided us with the idea that H^+-ATPase might function to provide a local acid environment around the cell membrane after lysosomes fuse to the plasma membrane. Therefore a quite reasonable hypothesis is that lysosomal trafficking upon FasL stimulation results in H^+-ATPase accumulation in the cell membrane, which pumps protons outside the cells and provides a hospitable environment for the ASM, thereby promoting the clustering of MRs.

The present study was designed to test this hypothesis. First, we analyzed the effects of local pH change on MR raft clustering and NADPH oxidase activity in CAECs. Second, we tested whether local endogenous pH around ECs was changed by FasL stimulation, using the pH indicator dye OG488 added to the tissue chamber with cells immobilized in Matrigel. Then, in addition to the use of the inhibitors of lysosome fusion, some inhibitors targeting H^+-ATPase were applied to examine their effects on FasL-induced change in local pH. Furthermore, we investigated whether H^+-ATPase protein can be translocated into the cell membrane accompanying lysosomal fusion into the cell membrane. All these experiments attempted to demonstrate that the translocated lysosomal H^+-ATPase exerts a critical local influence on the extracellular pH, which facilitates the formation and activation of MR redox-signaling signalosomes that are associated with ASM in coronary endothelial cells.

RESULTS

Effects of pH changes on local ceramide production and MR clusters

Fluorescence microscopy is often used to study cell MRs. For example, fluorophores conjugated to cholera toxin B subunit can bind to the raft constituent ganglioside GM1. In the present study, Alexa 488–cholera toxin B (Al488-CtxB) was used to label MRs. Under resting condition, there was only some diffuse fluorescent staining on the cell membrane stained by Al488-CtxB (Figure 1A, Ctrl), indicating an even distribution of single MRs without clusters. When the cells were incubated with FasL for 15 min, large fluorescent dots or patches were detected on the cell membrane. These fluorescent patches indicate the possible formation of MR clusters or macrodomains. In addition, MR clustering and colocalization with ceramide

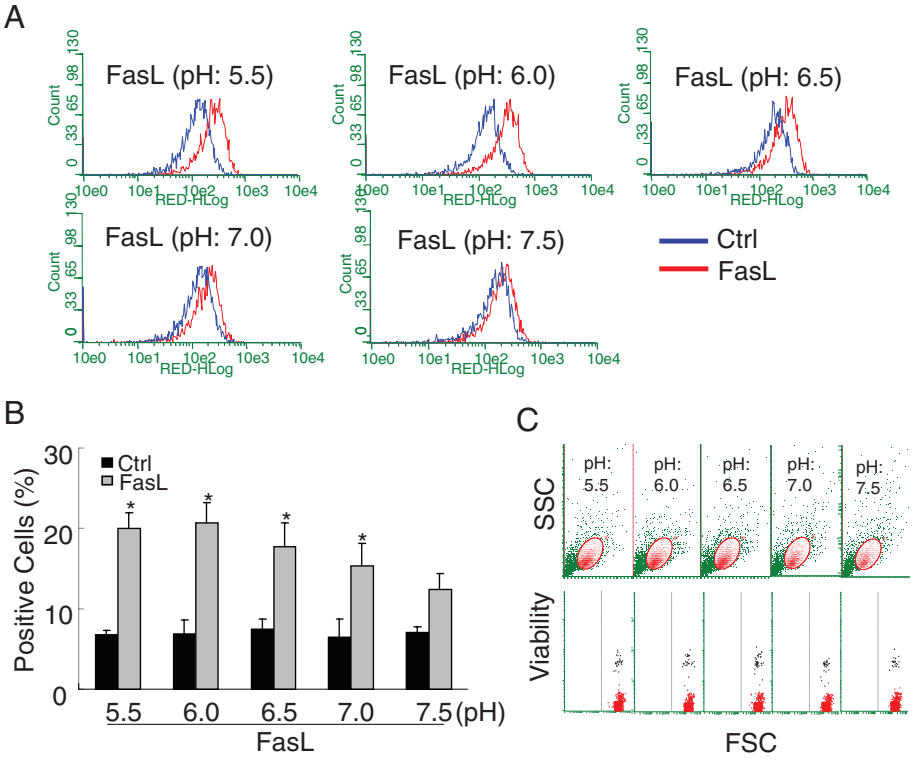

FIGURE 2: Measurements of ceramide in bovine CAECs by flow cytometry. (A) Frequency histogram of ceramide in control and FasL-treated cells exposed to pH 5.5, 6.0, 6.5, 7.0, and 7.5. (B) The percentage of ceramide positive-staining cells increased due to FasL treatment under different pH conditions. At pH 6.0, the percentage reached the maximum (n = 6, *p < 0.05 vs. control). (C) Top, no significant change of forward and side scatter under different pH conditions, which suggests that the treatment has no effect on cell size or granularity. Bottom, cell viability measured by flow cytometry. Cells were stained by ViaCount reagent. Viable cells appear at the bottom and dead cells at the top. The results show that the viability was not <95% under different pH conditions.

was significantly blocked by the MR disruptor methyl-β-cyclodextrin (MCD; Supplemental Figure S1), which confirmed that MR clustering is involved in the stimulation of FasL. To test the role of pH changes, the medium pH of the culture medium was adjusted to 5.5, 6.0, 6.5, 7.0, and 7.5, respectively, before addition of FasL. It was found that MR clusters increased when the pH of the bath solution was lowered. Figure 1B shows that the percentage of cluster positive cells stained by Al488-CtxB after FasL treatment significantly increased compared with control at all pH levels. The magnitude of the increases in MR clusters was much higher when the pH of the bath solution was <6.0. In addition, our previous studies showed that the frequency histogram of CtxB staining was not right-shifted to higher fluorescence intensity when CAECs were treated with FasL (Bao *et al.*, 2010a). Thus FasL mainly produced MR clustering under different pH values without alteration of the amount of MRs on the cell membrane. In a colocalization study using Al488-CtxB and a Texas red–conjugated anticeramide antibody, ceramide production was found locally in MRs in response to FasL when the pH of the bath solution was in the range of 5.5–6.5 (Figure 1C). However, when the pH increased to 7.0 or 7.5, the colocalization was not detected. Figure 1D summarizes the results of the costaining of CAECs by Al488-CtxB and Texas red–conjugated anti-ceramide antibody. After the cells were treated with FasL, the percentage of cells with colocalization of MRs and ceramide staining dramatically increased when pH in the bath solution was <6.5 but was not increased significantly at pH ≥ 7.0.

Using flow cytometry with anti-ceramide antibody, we found that the frequency histogram of membrane surface ceramide was shifted to higher fluorescence intensity in a pH-dependent manner, with a maximum production of ceramide at pH of 6.0 (Figure 2A). These results are summarized in Figure 2B. In addition, through observation with forward and side scatter and viability analysis with ViaCount reagent, pH change was found to not affect cell size, granularity, or cell viability (Figure 2C). Liquid chromatography–mass spectrometry analysis of ceramide confirmed this pH-dependent difference in ceramide production on the cell surface in response to FasL stimulation (Figure 3A). Moreover, FasL-induced ceramide production was dependent on ASM, because inhibition of ASM blocked the FasL-induced increase in ceramide production (Figure 3B).

Extracellular pH changes affect FasL-induced $O_2^{-\cdot}$ production of CAECs

In previous studies, we demonstrated that FasL-induced MRs clustering resulted in the formation of redox signaling platforms associated with increased NADPH oxidase activity and production of $O_2^{-\cdot}$ (Bao *et al.*, 2010a). Therefore we measured $O_2^{-\cdot}$ as a functional parameter in response to FasL stimulation at different pH values. In these experiments, NADPH-dependent $O_2^{-\cdot}$ production was measured by 1-hydroxy-3-methoxycarbonyl-2,2,5,5-tetramethylpyrrolidine (CMH) trapping after incubation of the cells with NADPH as substrate. The superoxide dismutase (SOD)–inhibitable fraction of the signal specifically reflected NADPH-dependent $O_2^{-\cdot}$ production. Figure 4A depicts representative changes in the electron spin resonance (ESR) spectrometric curve recorded under control and FasL-treated conditions. It was clear that the spectra of CMH-trapped $O_2^{-\cdot}$ markedly increased in response to FasL, with a higher production rate at lower pH of the bath solution. As summarized in Figure 4B, a rapid increase in $O_2^{-\cdot}$ production stimulated by FasL was observed in a pH-dependent manner compared with control. At extracellular pH of 6.0, FasL-induced $O_2^{-\cdot}$ production reached a maximum. When pH increased to 7.5, FasL-induced $O_2^{-\cdot}$ production was significantly reduced compared with that at pH 6.0. In addition, compared with control, FasL markedly increased the $O_2^{-\cdot}$ production, which was inhibited after the pretreatment with membrane raft inhibitor MCD (Supplemental Figure S2). This confirmed that MR clustering is involved in the effect of FasL.

Role of lysosomal enzymes in MRs

To demonstrate the contribution of lysosome-derived enzymes to pH-dependent MRs, we first tested the involvement of lysosomes in the fluorescent patches. FasL stimulated MRs and ceramide aggregation. When the lysosome fusion inhibitor vacuolin-1 was used to pretreat the cells, FasL-induced MRs and ceramide aggregation were completely blocked. Similarly, when the lysosomal enzyme ASM was inhibited by its small interfering RNA (siRNA) or inhibitor

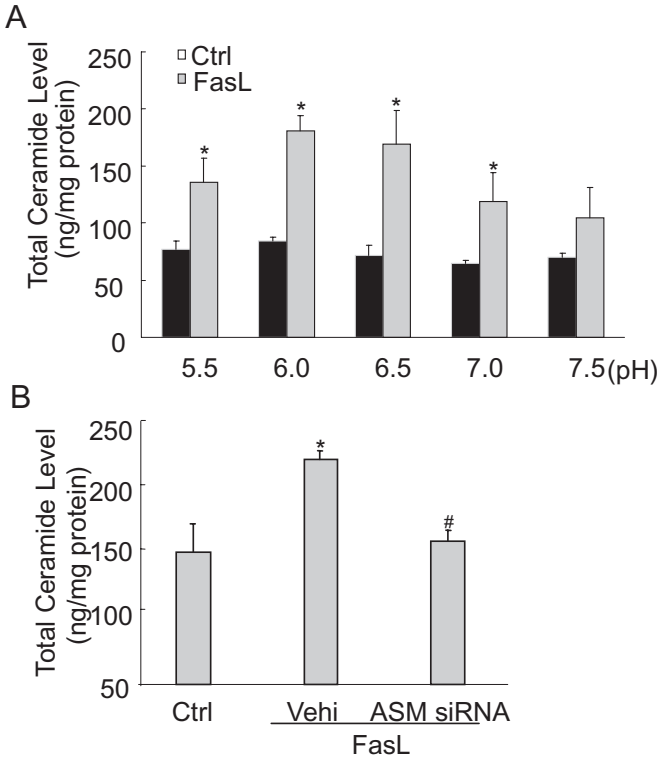

FIGURE 3: Measurement of ceramide concentration by liquid chromatography electrospray ionization tandem mass spectrometry. (A) Ceramide concentration in CAECs was increased due to FasL treatment under different pH conditions. Moreover, ceramide reached a maximum at pH 6.0. (B) ASM siRNA transfection significantly blocked the FasL-induced increase in ceramide production. (n = 4, *p < 0.05 vs. control; #p < 0.05 vs. only FasL-treated group).

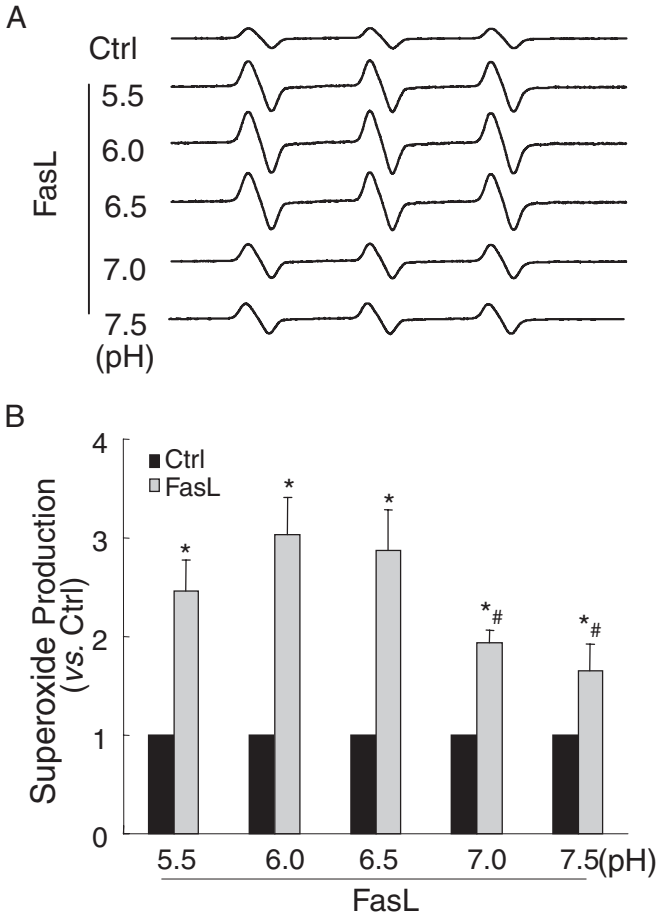

FIGURE 4: ESR spectrometric analysis of $O_2^{-\cdot}$ production in bovine CAECs stimulated by FasL. (A) Representative ESR spectrographs of $O_2^{-\cdot}$ trapped by CMH using NADPH as substrate. (B) Summary of data showing that $O_2^{-\cdot}$ production following FasL treatment (10 ng/ml) markedly increased and gradually decreased as the extracellular pH increased from 6.0 to 7.5 (n = 6, *p < 0.05 vs. control; #p < 0.05 vs. pH = 6.0 group).

Ami, both MRs and aggregated ceramide induced by FasL were no longer observed, even though the pH of the bath solution was maintained at 6.0. Lysosomal H^+-ATPase subunit of V1 sector (V1 H^+-ATPase) siRNA or its inhibitor also substantially inhibited FasL-induced MRs and ceramide aggregation. These results are summarized in Figure 5A, showing that the colocalization coefficient of MRs and ceramide was significantly increased after stimulation of the cells with FasL. Vacuolin-1 is a nonspecific inhibitor of lysosomal fusion, and bafilomycin A1 (Baf) is a macrolide antibiotic that specifically inhibits the V0 subunit of H^+-ATPase. When the cells were pretreated with vacuolin-1, the ASM siRNA or ASM inhibitor Ami, or the lysosomal V1 H^+-ATPase siRNA or Baf, FasL failed to induce any MRs and ceramide aggregation in the membrane of CAECs.

In addition, membrane fraction flotation analysis detected positive expression of flotillin-1, a component and marker of MRs, in fractions 3–5, which were referred to as MR fractions previously (Shao *et al.*, 2003). Figure 5B shows that V1 H^+-ATPase could be detected in membrane raft fractions in CAECs. A marked increase in V1 H^+-ATPase protein in MR microdomains was observed when CAECs were stimulated by FasL. This increase was significantly attenuated by pretreatment with V1 H^+-ATPase siRNA.

H^+-ATPase in FasL-induced changes in extracellular pH and intracellular $O_2^{-\cdot}$

In these experiments, dihydroethidine (DHE) was loaded into the cells to detect the level of intracellular $O_2^{-\cdot}$ Level, and OG488 was added into Matrigel solution to monitor extracellular pH changes around the cells. Measurement of $O_2^{-\cdot}$ reflects FasL-induced raft-redox signaling, as we demonstrated in previous studies (Bao *et al.*, 2010a). Figure 6A presents typical fluorescent images showing changes in extracellular pH (from blue to yellow) and intracellular $O_2^{-\cdot}$ (from light red to dark red within the cell). A rapid change in pH outside the cells in response to FasL was observed, as shown in acquired images at time points of 0, 3, 6, and 12 min following addition of FasL. In the presence of V1 H^+-ATPase siRNA or its inhibitor Baf, FasL no longer increased intracellular or extracellular fluorescence. Figure 6B presents the summarized data illustrating pH changes and $O_2^{-\cdot}$ production in response to FasL under the control condition and with H^+-ATPase inhibitor or its siRNA. Under the control condition or when CAECs were treated with scrambled sRNA, FasL time dependently increased OG488 fluorescence, meaning reduction in pH outside these cells, whereas intracellular $O_2^{-\cdot}$ levels increased in parallel. However, these changes in extracellular pH and intracellular $O_2^{-\cdot}$ levels induced by FasL were substantially attenuated by pretreatment of the cells with either H^+-ATPase inhibitor Baf or its siRNA. In addition, MCD significantly inhibited FasL-induced changes in extracellular pH and intracellular $O_2^{-\cdot}$ production in CAECs, which suggested that MR clustering induced by FasL is involved in these changes in extracellular pH and intracellular $O_2^{-\cdot}$ levels (Supplemental Figure S3).

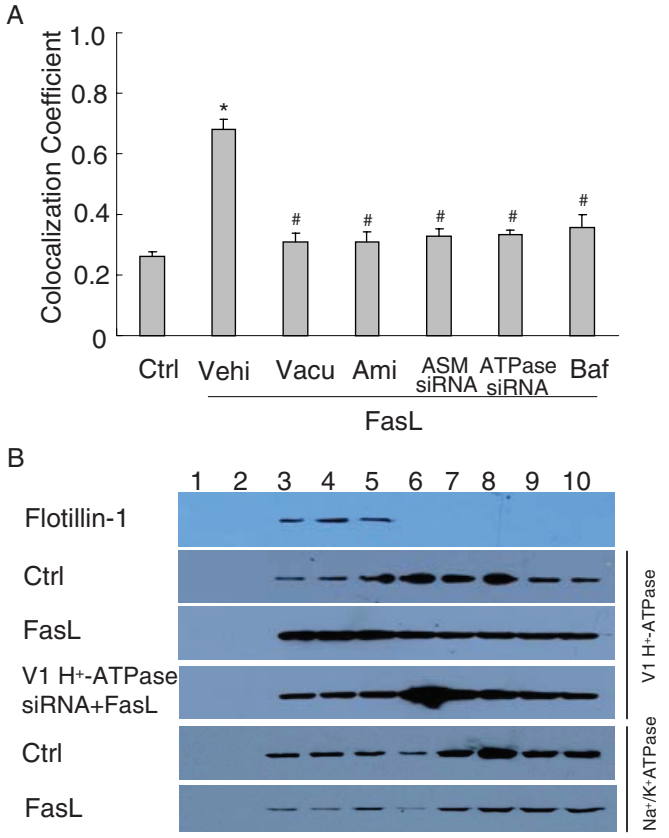

FIGURE 5: Effects of lysosome fusion inhibition on the CtxB-staining fluorescent patches and ceramide. (A) Percentage changes in positive cells costained by Al488-CtxB and anticeramide antibody in FasL-stimulated CAECs pretreated with lysosome fusion inhibitor vacuolin-1 (10 μM), ASM inhibitor Ami (20 μM), ASM siRNA, V1 H^+-ATPase siRNA, and its inhibitor Baf (100 nM). ($n = 6$, $p < 0.05$ vs. control; $^{\#}p < 0.05$ vs. only FasL-treated group). (B) Distribution and localization of H^+-ATPase as a MR redox platform on the membrane in CAECs treated with FasL alone or with FasL after pretreatment of V1 H^+-ATPase siRNA. Fractions 3–5 were designated as MRs, as indicated by the marker protein flotillin-1. The blot pattern for H^+-ATPase represents four individual experiments. Na^+/K^+-ATPase could also be detected in membrane raft fractions. However, no marked increase in the Na^+/K^+-ATPase protein in MR microdomains was observed in FasL-treated CAECs.

Lysosome fusion required for FasL-induced changes in extracellular pH and intracellular $O_2^{\cdot-}$

To determine whether the FasL-induced extracellular pH decrease or intracellular $O_2^{\cdot-}$ increase is associated with lysosome fusion, we tested the effects of siRNA or chemical lysosome fusion inhibitors on the changes in extracellular pH and intracellular $O_2^{\cdot-}$. Tetanus toxin is a special inhibitor of soluble *N*-ethylmaleimide–sensitive factor attachment protein receptor (SNARE) inhibitor. As shown by the typical fluorescence images presented in Figure 7A, lysosome fusion inhibition by tetanus toxin, vacuolin-1, or target-SNARE siRNA (Vamp-2 siRNA) almost completely blocked FasL-induced reduction of extracellular pH and increase in intracellular $O_2^{\cdot-}$ production compared with that observed under control condition or after treatment with scrambled small RNA (sRNA). Figure 7B summarizes these results. Under the control condition or when CAECs were treated with scrambled sRNA, FasL time dependently increased OG488 fluorescence, meaning the pH outside the cells decreased, whereas the intracellular $O_2^{\cdot-}$ level increased. This parallel decrease in extracellular pH and increase in intracellular $O_2^{\cdot-}$ level induced by FasL was significantly attenuated by inhibition of lysosome fusion using tetanus toxin, vacuolin-1, or Vamp-2 siRNA.

Lysosome fusion–dependent translocation of H^+-ATPase

As shown in Figure 8A, after stimulation with FasL the frequency histogram of H^+-ATPase as measured by cytometry was right-shifted to higher fluorescence intensity, suggesting recruitment of the protein into the cell membrane. In the presence of lysosome fusion inhibitor vacuolin-1 or tetanus toxin, the aggregation of V1 H^+-ATPase protein was effectively suppressed. These results are summarized in Figure 8B. The percentage of positive-staining cells with anti-V1 H^+-ATPase was significantly increased by FasL, an effect that was substantially attenuated by vacuolin-1 or tetanus toxin. It appears that V1 H^+-ATPase proteins are translocated to the cell membrane after activation by FasL and that lysosomal fusion mediates this translocation. In fluorescence resonance energy transfer (FRET) experiments, V1 H^+-ATPase was found translocated into the cell membrane from lysosomes, because the FRET (blue images) between V1 H^+-ATPase and ganglioside GM1 (CtxB labeling) or ASM increased upon FasL stimulation (Figure 9A). These results are summarized in Figure 9B, showing that the FRET efficiency between V1 H^+-ATPase and ASM or GM1 significantly increased in response to FasL stimulation. Pretreatment of these CAECs with lysosome fusion inhibitor vacuolin-1 and V1 H^+-ATPase siRNA remarkably decreased the FRET efficiency.

Lysosome fusion–dependent H^+-ATPase activity on the membrane of CAECs

Bafilomycin-sensitive H^+-ATPase activity on the CAEC membrane is shown in Figure 10A. H^+-ATPase activity was significantly enhanced upon FasL stimulation for 15 min. In the presence of vacuolin-1, the FasL-induced enhancement of H^+-ATPase activity was significantly blocked. Similar results were obtained by another lysosome fusion inhibitor, tetanus toxin or V1 H^+-ATPase siRNA. Of interest, V1 H^+-ATPase siRNA had no effect on H^+-ATPase activity in the absence of FasL stimulation. It is likely that the surface activity as measured in that assay reflects an activity other than that of the H^+-ATPase to which the siRNA is directed. Furthermore, cell surface biotinylation assay showed that V1 H^+-ATPase protein was increased by 59.5% on the cell membrane when BCAECs were treated with FasL, which suggested that ~59.5% of the total V1 H^+-ATPase may be externalized to cell membrane due to FasL treatment. In addition, ASM or lysosomal-associated membrane protein 1 (Lamp-1) are regarded as control of the relocalization of lysosomal protein to the cell surface, and it was found that the intensity ratio of ASM or Lamp-1 to transferrin receptor increased by 67.1 or 47.7%, respectively, on the cell membrane (Figure 10, B and C).

DISCUSSION

The present study found that MR clustering decreases when pH becomes neutral or slightly alkaline. Consistent with such changes in MR clustering, the colocalization of MR and the ASM product ceramide is reduced when extracellular pH increases. In addition, the results from flow cytometry and ceramide quantification further demonstrate that FasL-induced MR clustering contributes to the production of ceramide in the cell membrane at low extracellular pH level. Moreover, both confocal and flow cytometric analyses show that pH 6.0 is an optimum condition for intensive MR cluster formation. These results suggest that ASM-associated MR clustering depends on a low-pH microenvironment around the ECs.

Our previous studies showed that MR clustering is an important mechanism determining the trafficking and aggregation of NADPH

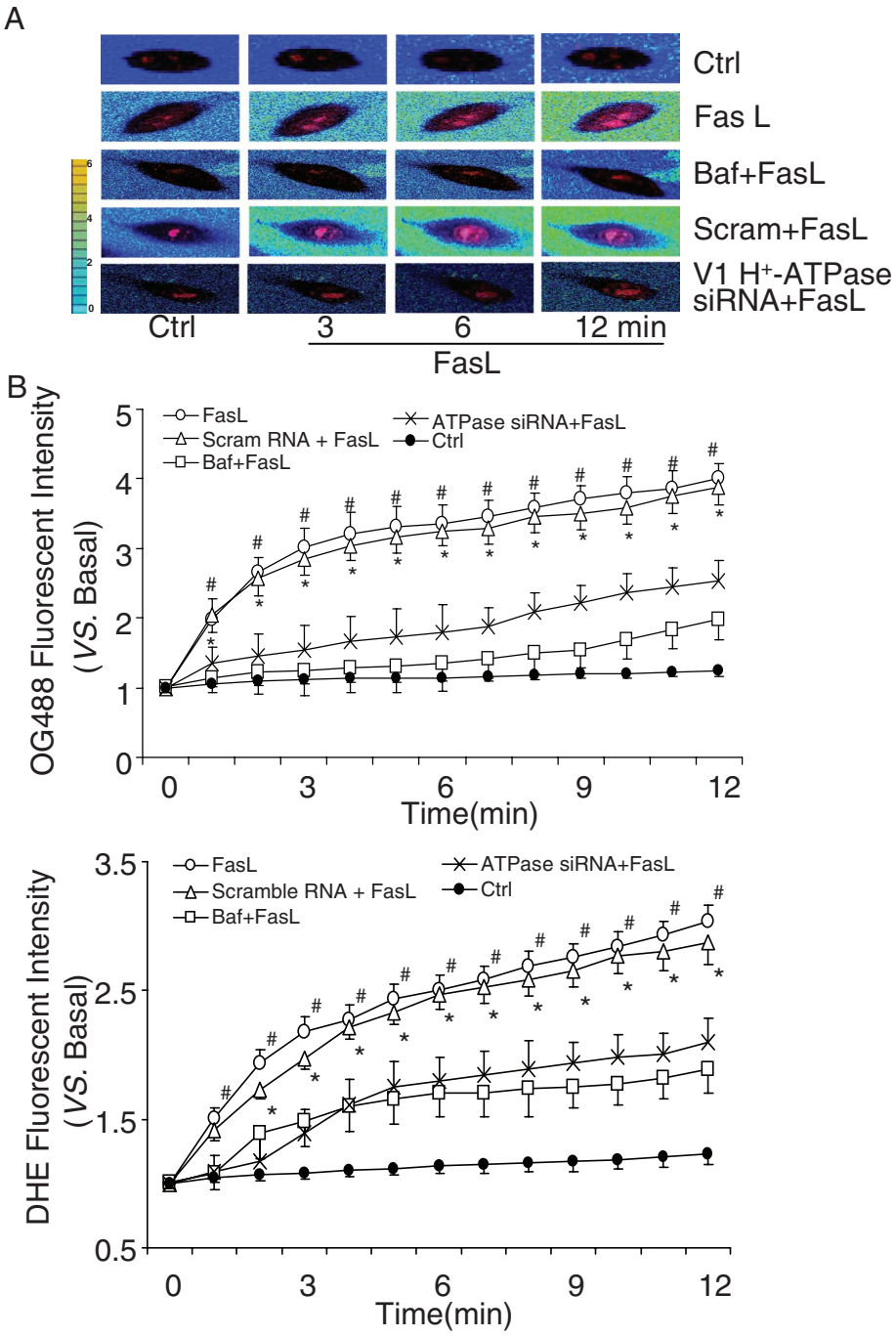

FIGURE 6: Role of lysosomal H+-ATPase in extracellular pH and $O_2^{-\cdot}$ production in bovine CAECs. (A) Typical merged images of OG488 and DHE fluorescence using an Olympus scanning confocal microscope at excitation/emission of 480/610 nm and 495/524 nm. The change of OG488 fluorescence intensity was recorded with pseudo color, which shows blue to green and then to yellow with increasing fluorescence intensity. (B) Summary of data showing that treatments with Baf (100 nM) or V1 H+-ATPase siRNA significantly inhibited FasL-induced changes in extracellular pH and intracellular $O_2^{-\cdot}$ production in CAECs (n = 6, *p < 0.05 vs. V1 H+-ATPase siRNA–treated group; #p < 0.05 vs. Baf-treated group).

oxidase subunits in the cell membrane of endothelial cells (Jin *et al.*, 2008b). In addition, lysosome-targeted ASM is able to traffic to and become exposed on the cell membrane surface, which may lead to MR clustering and NADPH oxidase activation in CAECs (Bao *et al.*, 2010a). In this process, the role of local extracellular pH change in the activity of NADPH oxidase remained unclear. The present study showed that that an acidic pH is important for the activation of lysosomal enzymes and MR cluster formation. This action of pH on MR cluster formation has a profound effect on NADPH oxidase activity (Mantegazza *et al.*, 2008). As measured by ESR, NADPH oxidase activity stimulated by FasL in CAECs is highly sensitive to extracellular pH, which is consistent with MR clustering that varies with different pH. Although there are a number of reports indicating that NADPH oxidase may work in a pH-dependent manner with an optimum near pH 6.0 (Henderson, 1998; DeCoursey *et al.*, 2001; Schwarzer *et al.*, 2004), these studies did not associate such pH dependence with MR clustering.

One of the important findings from the present study is that local pH changes around the cell membrane of CAECs upon stimulation by FasL are determinants for MR clustering and formation of MR redox signalosomes. The synchronous change between local extracellular pH change and intracellular $O_2^{-\cdot}$ production further demonstrated that MR clustering due to pH changes is associated with NADPH oxidase activity. This local acidic microenvironment is important for the activation of the MR redox signaling in these cells, as shown by intracellular $O_2^{-\cdot}$ production.

The next question we tried to answer was what mechanism mediates the FasL-induced pH decrease outside these CAECs. In previous studies, we identified that lysosomes were fused with the cell membrane upon FasL stimulation, leading to the translocation of ASM (Jin *et al.*, 2008a; Bao *et al.*, 2010b). Moreover, lysosomal trafficking was important in MR clustering in EC membranes, leading to the formation of signaling platforms (Jin *et al.*, 2008a). The present study further demonstrated that the fusion and function of lysosomes was involved in FasL-induced pH decrease and MR redox activation in response to FasL, as shown by the blocking effect of the lysosomal fusion inhibitors on the FasL-induced pH decrease. In addition, we found that the microtubule-depolymerizing reagent nocodazole can inhibit the fluorescent destaining of lysosomal dye FM2-10, which suggested that microtubules play a role in lysosomal relocation to the cell membrane in response to FasL (Supplemental Figure S4). To our knowledge, these results provide the first evidence that lysosomal fusion leads to a local pH reduction and thereby determines MR clustering and redox signaling activation.

To further explore the mechanisms mediating the formation of a local acidic environment for ASM around the cell membrane during FasL stimulations, we addressed the role of H+-ATPase. Given the fact that H+-ATPase pumps protons from the cytoplasma into lysosomes (Jefferies *et al.*, 2008; Tabata *et al.*, 2008), outward proton flux may occur, because the inner member of lysosomes often faces outside the cells. In addition, some factors are reported to participate in the regulation of pH. For example, it was reported that the generation

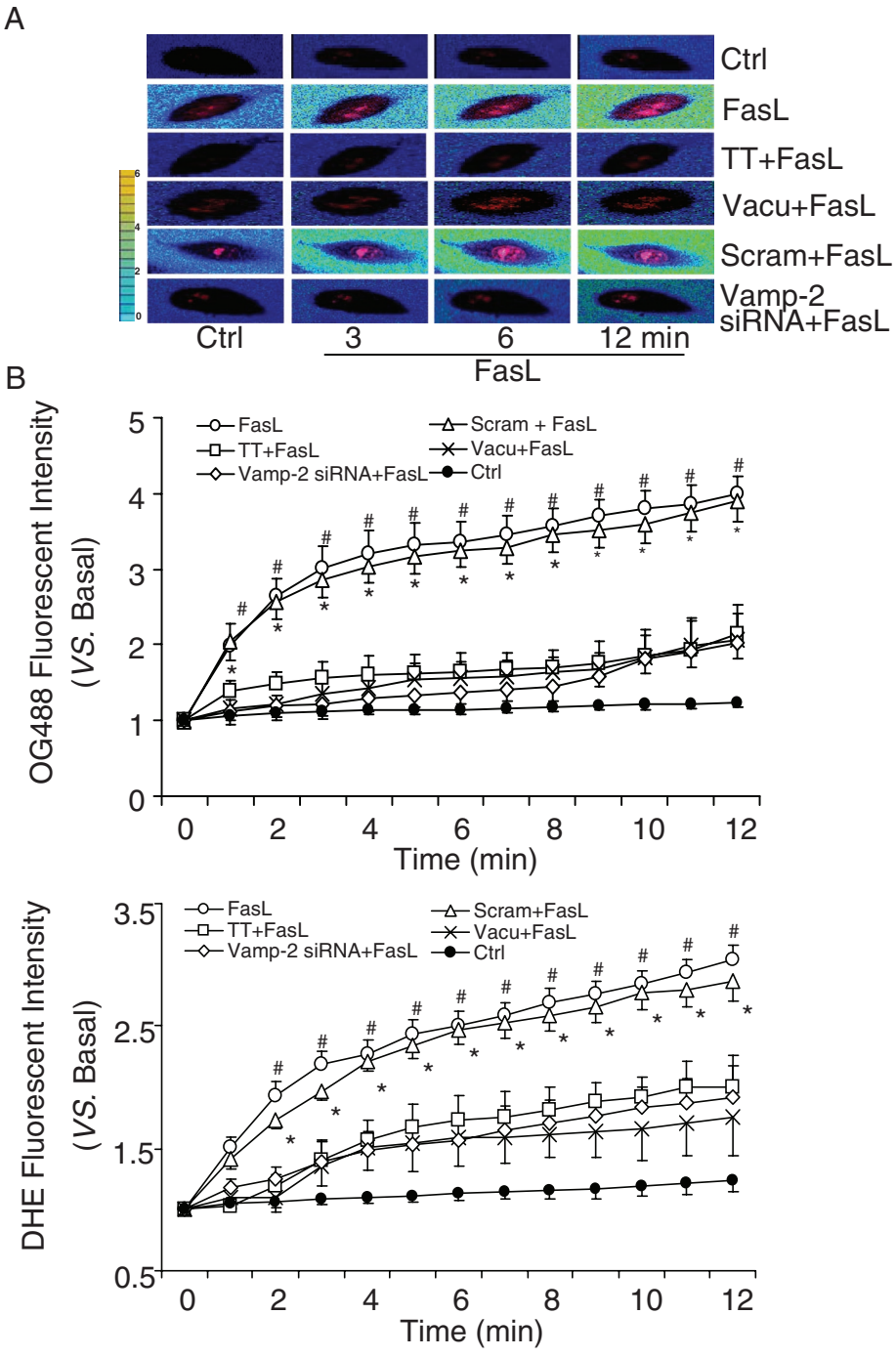

FIGURE 7: Effects of lysosomal fusion on extracellular pH and intracellular $O_2^{-\cdot}$ production in bovine CAECs. (A) Typical merged images of OG488 and DHE fluorescence. The change of OG488 fluorescence intensity was recorded in pseudo color. (B) Summary of data showing that TT (10 nM), vacuolin-1 (10 μM), and vamp-2 siRNA significantly inhibited FasL-induced changes in extracellular pH and intracellular $O_2^{-\cdot}$ production in CAECs (n = 6, *p < 0.05 vs. Vamp-2 siRNA–treated group; #p < 0.05 vs. vacuolin-1 or TT-treated group).

of $O_2^{-\cdot}$ by NADPH oxidase is accompanied by the efflux of H^+ ions through the H^+ channel, which acts as the charge compensation pathway for the electrogenic generation of $O_2^{-\cdot}$ (Henderson, 1998). In addition, interference of the α4 isoform of Na^+/K^+-ATPase with ouabain causes a pH decline of sperm cytoplasm through functional coupling to the Na^+/H^+ exchanger (Jimenez *et al.*, 2010), and protein kinase C–mediated phosphorylation of rat α1 Na^+/K^+-ATPase alters pH in COS cells (Belusa *et al.*, 1997). However, the present study demonstrated that bafilomycin A1 resulted in a failure of FasL to reduce the extracellular local pH. V1 H^+-ATPase siRNA was also found to eliminate FasL-induced pH decrease outside CAECs. Thus our data suggest that V1 H^+-ATPase rather than NADPH oxidase–associated H^+ channel or Na^+/K^+-ATPase coupling with Na^+/H^+ exchanger plays a major role in H^+ transportation in the EC membrane.

Recent studies indicate that ASM can be acidified in lysosomes depending on luminal pH prior to fusion of the vesicles. It was reported that in hepatocytes, hyperosmotic exposure induces an almost instantaneous acidification of ASM-containing endosomal compartment, which is followed by an increase in the intracellular ceramide concentration (Reinehr and Haussinger, 2007; Lang *et al.*, 2011). Moreover, inhibition of the vacuolar-type H^+-ATPase abolishes not only endosomal acidification and subsequent ceramide generation, but also hyperosmotically induced generation of ROS by NADPH oxidase. The present study suggests that when lysosome fuses with cell membrane, translocated lysosomal V1 H^+-ATPase provides an acid environment, which maintains the activation of membrane acid sphingomyelinase to magnify the production of ceramide. Taken together, these data suggest a model in which ASM is activated in the lysosome to initialize the ceramide production in the lysosome; once ASM is translocated in the plasma membrane, translocated lysosomal V1 H^+-ATPase provides a microenvironment with acidic pH, which is critical to sustain the ASM activity for production of a large amount of ceramide and consequent formation of ceramide-enriched membrane platforms.

Additional experiments were performed to determine whether H^+-ATPase stems from translocated lysosomes induced by FasL. Using flow cytometry, it was confirmed that this FasL-induced translocation of V1 H^+-ATPase mainly stemmed from lysosomes because V1 H^+-ATPase–positive staining of cells was substantially blocked by vacuolin-1 and tetanus toxin. By confocal microscopy, V1 H^+-ATPase was also found to be translocated into the MR clusters when CAECs were stimulated by FasL, which was significantly inhibited by treatment with either vacuolin-1 or V1 H^+-ATPase siRNA. FRET analysis demonstrated that V1 H^+-ATPase and ASM are very closely localized after they are translocated to the cell MR areas. This suggests that lysosomal V1 H^+-ATPase is not only aggregated in the cell membrane upon FasL stimulations, but also is assembled into an MR signalosome complex to function as a signaling platform. It was reported that MR-like domains also plays a role in regulating the activity of the H^+-ATPase pump (Lafourcade *et al.*, 2008). It is plausible that there is a feedforward loop for H^+-ATPase aggregation in membrane raft and

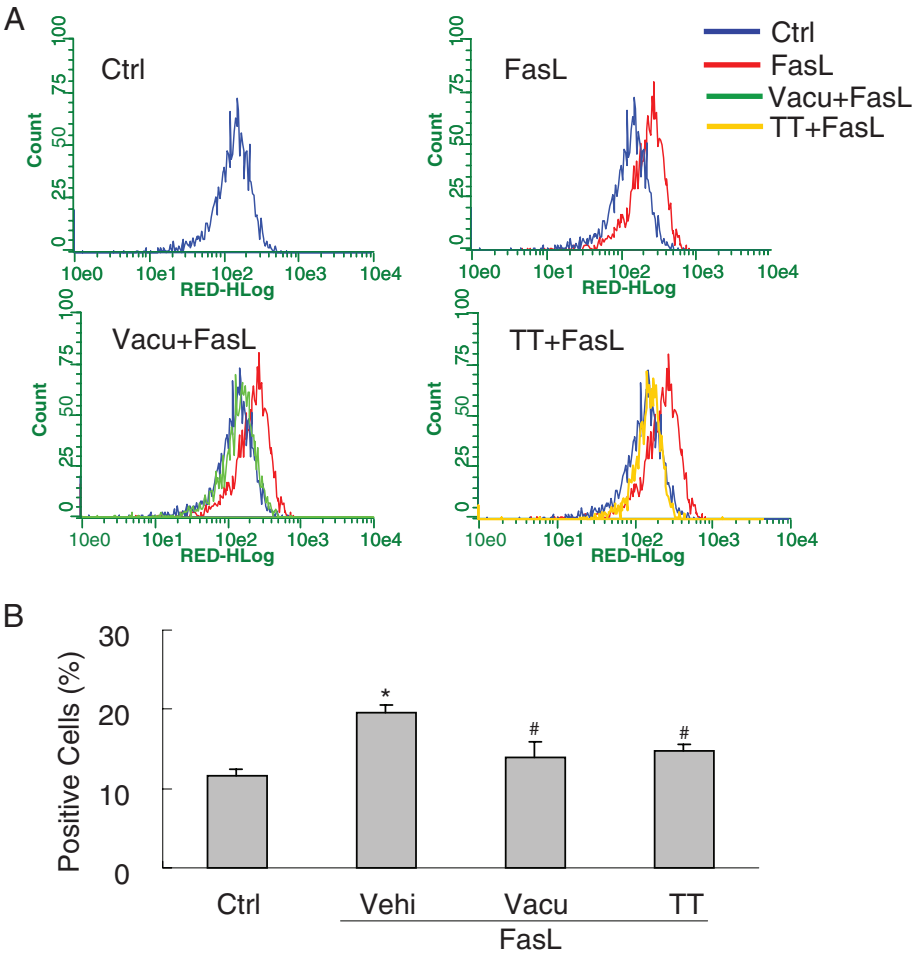

FIGURE 8: Measurements of H⁺-ATPase translocation in bovine CAECs with flow cytometry. (A) Frequency histogram of H⁺-ATPase in the membranes of control or FasL-stimulated (10 ng/ml for 15 min) cells without or with TT (10 nM) or vacuolin-1 (10 μM) and the overlay. (B) The percentage of H⁺-ATPase positive–staining cells significantly increased in FasL-treated CAECs, which was suppressed by preincubation with vacuolin-1 or TT (n = 6, *p< 0.05 vs. control; #p < 0.05 vs. only FasL-treated group).

membrane raft clustering. In this model, upon stimulation, lysosomal fusion with the plasma membrane results in exposure of H⁺-ATPase in the plasma membrane, which is crucial for ASM activation, ceramide production, and consequent formation of ceramide-enriched membrane platforms. H⁺-ATPase aggregation in MR platform may enhance the acidic microenvironment around this platform and thus enhance ASM activity, which promotes the formation of larger, ceramide-enriched signaling platforms and amplifies raft-associated signals. The activity of H⁺-ATPase activity is critical for the activity of ASM to produce ceramide-enriched MR clusters and consequent redox signaling platforms. This enhanced H⁺-ATPase activity by FasL treatment was indeed demonstrated by biochemical analysis. Furthermore, it was suggested that the membrane H⁺-ATPase activity in these cells is due to the its translocation via lysosome fusion.

In conclusion, FasL stimulation leads to a local acid microenvironment around the CAEC membrane, which facilitates the activity of ASM and enables consequent formation of MR redox signal platforms. The activation of translocated V1 H⁺-ATPase via lysosome fusion serves as a proton pump and functions to keep such locally acidic region for the activity of ASM, leading to ceramide production and MR clustering, which promotes the formation of membrane redox signalosomes and thereby significantly participates in the regulation of endothelial function in the coronary circulation.

MATERIALS AND METHODS

Cell culture

Primary cultures of bovine CAECs were obtained as described previously (Zhang *et al.*, 2006; Jin *et al.*, 2008b). All studies were performed with CAECs of two to four passages.

RNA interference of ASM, Vamp-2, and H⁺-ATPase

The siRNAs were designed with BLOCK-iT RNAi Designer (Invitrogen Life Science, Grand Island, NY). The DNA target sequence for H⁺-ATPase siRNA is 5′-CACAGCGAGUUGGUUGGAGAGAUUA-3′; ASM siRNA is 5′-AAGGCCGTGAGTTTCTACCT-3′; and Vamp-2 siRNA is 5′-CAUCAUCGUUUACUUCAGCUCUUAA-3′; and the scrambled small RNA (AATTCTCCGAACGTGTCACGT) was confirmed as nonsilencing double-stranded RNA and used as control. Transfection of siRNA was performed using the TransMessenger transfection kit (Qiagen, Valencia, CA) according to the manufacturer's instructions. In view of the role of the H⁺-ATPase V1 subunit in traffic (Oehlke *et al.*, 2011), V1 subunit E1 mRNA (locus, NM_001079613) and its cDNA were chosen to design H⁺-ATPase siRNA. V1 H⁺-ATPase siRNA was confirmed to be effective in silencing H⁺-ATPase gene and protein expression through Western blot, PCR, and immunocytochemistry (Supplemental Figure S5). The siRNAs of ASM and Vamp-2 were confirmed to be effective in silencing ASM and Vamp-2 gene expression in our lab (Zhang *et al.*, 2007; Han *et al.*, 2011).

Confocal microscopy of the colocalization of MR clusters and ceramide

For dual-staining detection of the colocalization of MR marker with ceramide or V1 H⁺-ATPase, the CAECs were first incubated with Al488-CtxB, as described previously (Zhang *et al.*, 2006), and then, as needed, with mouse anti-ceramide immunoglobulin M (IgM) antibody (1:200; Alexis Biochemicals, San Diego, CA), which was followed by Texas red–conjugated anti-mouse secondary antibody (Molecular Probes, Eugene, OR). Then the colocalizations were visualized by confocal microscopic analysis. In addition, CtxB cluster–positive cells were counted from a total of 50 cells under a fluorescence microscope. Then the percentage changes of CtxB cluster–positive cells were calculated.

Flow-cytometric analysis of ceramide generation and H⁺-ATPase translocation on the cell membrane

The expression of ceramide and V1 H⁺-ATPase on the cell membrane was also assessed by flow cytometry. As described previously (Varsano *et al.*, 1998), CAECs were harvested and washed with phosphate-buffered saline (PBS) and then blocked with 1%

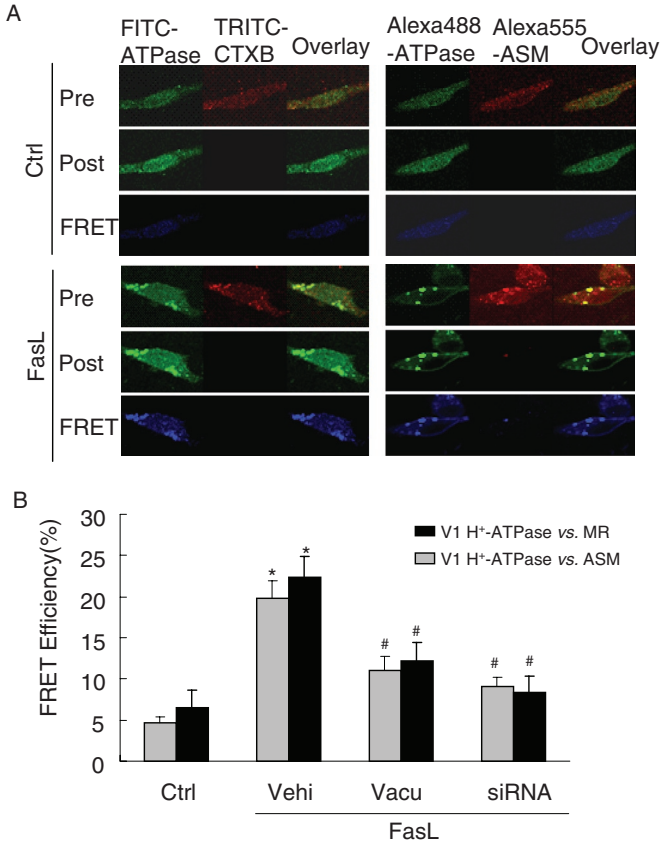

FIGURE 9: FRET analysis of the MR marker ganglioside GM1, H^+-ATPase, and ASM in bovine CAECs. FRET was detected using an acceptor-bleaching protocol. The blue images (representing FRET) on the bottom were obtained by subtracting a prebleaching image from a postbleaching image. (A) Representative images of FRET between V1 H^+-ATPase and GM1 (CtxB labeling) or ASM. (B) Summarized results of detected FRET efficiency show that FasL significantly increased the FRET efficiency between V1 H^+-ATPase and GM1 or ASM, which was effectively inhibited by vacuolin-1(10 μM) or V1 H^+-ATPase siRNA (n = 6, *p < 0.05 vs. control; #p < 0.05 vs. only FasL-treated group).

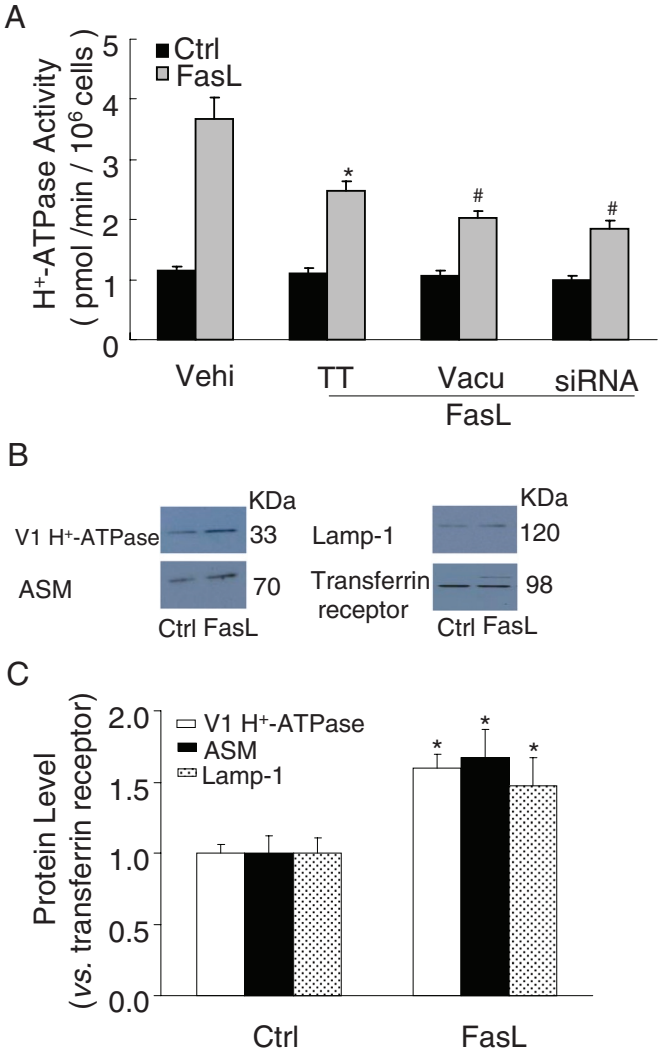

FIGURE 10: H^+-ATPase activity and protein expression on the cell membrane of bovine CAECs. (A) FasL (10 ng/ml) dramatically enhanced the activity of H^+-ATPase on the cell membrane of CAECs by fluorometry, which was inhibited by pretreatment of these cells with TT (10 nM), vacuolin-1 (10 μM), or V1 H^+-ATPase siRNA (n = 6, *p 0.05 vs. control; #p < 0.05 vs. only FasL-treated group). (B) Cell surface biotinylation assay for H^+-ATPase subunit of V1 sector protein expression in bovine CAECs. Western blot gel document presents the relative levels of V1 H^+-ATPase, ASM, lamp-1, or transferrin receptor on the cell membrane of CAECs. (C) Summary of results showing that the intensity ratio of V1 H^+-ATPase to transferrin receptor increased by 59.5% on the cell membrane in response to FasL (10 ng/ml) treatment. The intensity ratio of ASM or Lamp-1 to transferrin receptor increased by 67.1 or 47.7%, respectively, on the cell member (n = 3, *p < 0.05 vs. control).

bovine serum albumin (BSA) for 10 min at 4°C. Cell viability assessed by trypan blue staining was always >96%. After two washes, the pellet was added to 100 ml of PBS and incubated with goat anti-V1 H^+-ATPase IgG (1:200) or mouse anti-ceramide IgM antibody (1:200), followed by incubation with fluorescein isothiocyanate (FITC)–labeled rabbit anti-goat secondary antibody (BD Biosciences PharMingen, San Diego, CA; 1:500) or Texas red–conjugated anti-mouse secondary antibody (Molecular Probes). Stained cells were run on a Guava Easycyte Mini Flow Cytometry System (Guava Technologies, Hayward, CA) and analyzed with Guava acquisition and analysis software (Guava Technologies).

Liquid chromatography electrospray ionization tandem mass spectrometry for quantitation of ceramide

The separation, identification, and quantitation of ceramide in CAECs were performed by liquid chromatography electrospray ionization tandem mass spectrometry. The high-performance liquid chromatography (HPLC) system was equipped with a binary pump, a vacuum degasser, a column heater, and an autosampler (Waters, Milford, MA). The HPLC separation was performed at 70°C on a reverse-phase C18 Nucleosil AB column (5 μm, 70 mm × 2 mm inside diameter) from Macherey Nagel (Düren, Germany). The mobile phase was a gradient mixture formed as described (Fillet *et al.*, 2002). The cell lipids were extracted according to previous studies (Yi *et al.*, 2004). To avoid any loss of lipids, the extraction procedure was performed using siliconized glassware. Mass spectrometric detection was carried out using a Quattro II quadrupole mass spectrometer (Micromass, Altrincham, United Kingdom) operating under MassLynx 3.5 and configured with a Z-spray electrospray ionization source. Source conditions were as described (Fillet *et al.*, 2002).

ESR detection of $O_2^{-\cdot}$

For detection of the $O_2^{-\cdot}$ production dependent on NADPH oxidase, cells were gently collected and resuspended with modified Krebs–4-(2-hydroxyethyl)-1-piperazineethanesulfonic acid buffer containing deferoximine (100 µmol/l; Sigma-Aldrich, St. Louis, MO) and diethyldithiocarbamate (5 µmol/l; Sigma-Aldrich). These mixtures, containing 1×10^6 cells, were mixed with 1 mM of the $O_2^{-\cdot}$-specific spin trap CMH in the presence or absence of manganese-dependent SOD (200 U/ml; Sigma-Aldrich). The mixtures were then loaded into glass capillaries and immediately analyzed for $O_2^{-\cdot}$ formation kinetics for 10 min in a Miniscope MS200 ESR spectrometer (Magnettech, Berlin, Germany) as described (Jin *et al.*, 2008b). The ESR settings were as follows: biofield, 3350; field sweep, 60 G; microwave frequency, 9.78 GHz; microwave power, 20 mW; modulation amplitude, 3 G; 4096 points of resolution; and receiver gain, 50 for cells. The results were expressed as the fold changes of the treatment group versus the control.

Flotation of membrane MR fractions

CAECs pretreated with vehicle or V1 H^+-ATPase siRNA were stimulated by FasL (10 ng/ml) for 15 min. To isolate LR fractions from the cell membrane, these cells were lysed in 1.5 ml of MBS buffer containing (in micromoles per liter) morpholinoethane sulfonic acid, 25; NaCl, 150; EDTA, 1; phenylmethylsulfonyl fluoride, 1; and Na_3VO_4, 1; and a mixture of protease inhibitors and 1% Triton X-100 (pH 6.5). Cell extracts were homogenized by five passages through a 25-gauge needle. Then homogenates were adjusted with 60% OptiPrep Density Gradient medium (Sigma-Aldrich) to 40% and overlaid with an equal volume (4.5 ml) of discontinuous 30–5% OptiPrep Density Gradient medium. Samples were centrifuged at 32,000 rpm for 24 h at 4°C using a SW32.1 rotor. Fractions were collected from the top to bottom. Then proteins in each fraction were precipitated by adding an equal volume of 30% trichloroacetic acid and incubating for 30 min on ice. Precipitated proteins were spun down by centrifugation at 13,000 rpm at 4°C for 15 min. The protein pellet was carefully washed twice with cold acetone, air dried, and resuspended in 1 mol/l Tris-HCl (pH 8.0) for Western blot. In addition, Na^+/K^+-ATPase, a cell membrane protein not considered to cluster with MRs, was used as a negative control in this experiment (Figure 5B).

Simultaneous confocal microscopic analysis of intracellular $O_2^{-\cdot}$ and extracellular pH in CAECs

To measure intracellular $O_2^{-\cdot}$ production in isolated vascular endothelial cells, we used a DNA-binding assay for $O_2^{-\cdot}$, which oxidizes exogenously added DHE to produce a strong red fluorescence. In these experiments, isolated CAECs (1×10^6 cells/well) were seeded into a 35-mm dish and incubated overnight to attach to the bottom of the wells. The cells were then pretreated with bafilomycin A1 (100 nM; Sigma-Aldrich), tetanus toxin (TT; 10 nM; Sigma-Aldrich), vacuolin-1 (10 µM; Sigma-Aldrich), amitriptyline (20 µM; Sigma-Aldrich), or siRNA of ASM, Vamp-2, or V1 H^+-ATPase before treating with FasL. On the day of experiments, the culture medium was first discarded, and CAECs were washed twice with PBS buffer, followed by addition of 1 ml of PBS containing DHE (10 µM; Invitrogen, Carlsbad, CA). After 30 min at room temperature, the DHE solution was discarded, and the cells were washed twice with fresh PBS and then overlaid with Matrigel containing OG488 (1 mM). The change of OG488 fluorescence intensity was recorded in pseudo color, which shows blue to green and then to yellow with increasing fluorescence intensity (Baader *et al.*, 2002). The staining of DHE for intracellular $O_2^{-\cdot}$ and OG488 for extracellular pH was visualized after treatment with FasL, respectively, using an Olympus scanning confocal microscope (Olympus, Tokyo, Japan) at excitation/emission of 480/610 nm and 495/524 nm. The merged image was shown as the final result. DHE and OG488 fluorescence intensity was analyzed with FluoView software, version 5.0. The ratio of fluorescence intensity to that at basal level was quantified to show $O_2^{-\cdot}$ level and pH change.

Fluorescence resonance energy transfer measurement

To determine the molecular complex in MR clusters, CAECs were stained with FITC-labeled anti-V1 H^+-ATPase antibody and then with tetramethylrhodamine isothiocyanate (TRITC)- labeled CtxB, Alexa 488–labeled anti-V1 H^+-ATPase antibody, or Alexa 555–labeled anti-ASM antibody. These cells were then visualized using confocal microscopy. An acceptor bleaching protocol was used to measure the FRET efficiency (Van Munster *et al.*, 2005; Nieminen *et al.*, 2007; Jin *et al.*, 2008a; Bao *et al.*, 2010b). After prebleaching images were taken, the laser intensity at an excitation wavelength of the acceptor (TRITC or Alex 555) was increased from 50 to 98 W/cm^2 and continued to excite the sample cells for 2 min to bleach the acceptor fluorescence. After the excitation intensity was adjusted back to 50 W/cm^2, the postbleaching image was taken. The FRET images were obtained by subtraction of the prebleaching image from the postbleaching image and are shown in blue. The FRET efficiency was calculated as described previously (Van Munster *et al.*, 2005; Nieminen *et al.*, 2007; Jin *et al.*, 2008a; Bao *et al.*, 2010b).

Assay for H^+-ATPase activity

The method for determination of H^+-ATPase activity is a modification of the assay for H^+-ATPase activity in microdissected tubule segments (Tojo *et al.*, 1994). ATPase activity was measured by a fluorometric method in which ATP hydrolysis was coupled to oxidation of NADH. Baf was used as a specific inhibitor of vacuolar H^+-ATPase. CAECs (1×10^6 cells/well) were seeded into a 35-mm dish and pretreated with vacuolin-1 prior to FasL stimulation for 15 min. Then the CAECs were harvested and resuspended in assay buffer containing (in mM) 100 NaCl, 66.7 NH_4Cl, 3.7 $MgC1_2$, 2 $CaC1_2$, 50 imidazole, 5 glucose, and 0.05% BSA. To each sample was added 20 µl of reaction solution 1 with or without bafilomycin. Reaction solution 1 contained (in millimoles) 100 NaCl, 66.7 NH_4Cl, 3.7 $MgCl_2$, 50 imidazole, 3.3 disodium ATP, 0.6 phosphoenopyruvate, 7.5 sodium azide, 12 ouabain, and 1 EDTA and 9.6 U/ml pyruvate kinase. All samples were divided into two groups—one without and the other with 30 nM bafilomycin. In the second group, reaction solution 1 containing 30 nM bafilomycin was added. After addition of reaction solution 1, the samples were incubated in a shaking water bath at 37°C for 40 min. The reactions were stopped by boiling the samples for 3 min. The amount of pyruvate generated during the first stage of the assay was determined by reacting the samples with 2.5 µM NADH and 6 U/ml lactate dehydrogenase in 1100 µl of 0.1 N potassium phosphate buffer (reaction solution 2), and the amount of NADH oxidized by pyruvate was measured by fluorometry. The excitation and emission wavelengths for NADH were 340 and 460 nm, respectively.

The bafilomycin-sensitive ATPase activity was defined as the difference in activity determined in the absence and presence of bafilomycin. The H^+-ATPase activity was expressed as pmol of ADP generated per min per 10^6 cells. The H^+-ATPase assay was performed under maximum reaction rate (V_{max}) conditions, as all reactants in the assay were added in considerable excess and ATP was being continuously regenerated during the assay. The only limiting factor was the generation of ADP from ATP by ATPases during the first stage of the assay. There was a 1:1 stoichiometric relationship between ADP formation during the first stage of the assay and NADH oxidation during

the second stage of the assay. Therefore a change in enzyme activity reflects a change in V_{max}, and changes in the kinetic properties of the enzyme because of putative changes in K_m for the substrate (ATP) or cofactors (Mg^{2+}) would not be detected under these conditions.

Cell surface biotinylation assay for expression of H^+-ATPase protein

As described previously (Perrotta *et al.*, 2010), cells (1×10^6 cells/well) were stimulated with 10 ng/ml FasL at the indicated times in culture medium at 37°C. Stimulation was stopped with ice-cold PBS. Cells were washed twice with PBS and then incubated twice with 0.5 mg/ml sulfo-NHS-LC-biotin in DMEM without serum for 10 min at 4°C. After washing with serum-free DMEM for 10 min and three times with PBS for 5 min at 4°C, cells were solubilized in lysis buffer (10 mM Tris, 150 mM NaCl, 1 mM EDTA, 0.1% SDS, and 1% Triton X-100 with protease inhibitor mixture, pH 7.4) for 30 min at 4°C. Lysates were then centrifuged for 5 min at 1500 × *g*, and streptavidin beads were added to the supernatant to isolate cell membrane proteins. After incubation of the mixture for 16 h at 4°C, biotin–streptavidin beads complexes were sedimented at 13,000 rpm for 3 min. The supernatant was used as control, and, after two washes with PBS, bead-bound proteins were denatured in Laemmli buffer and analyzed by SDS–PAGE, followed by Western blotting with the anti–V1 H^+-ATPase, anti–Lamp-1, or anti-ASM antibody. Lamp-1 and ASM is regarded as positive controls. Transferrin receptor was a conserved membrane protein used as a loading control in this study. Cell surface exposure of protein was normalized to 25 μg of total lysate for each sample.

Statistics

Data are presented as the mean ± SE. Significant differences between and within multiple groups were examined using analysis of variance for repeated measures, followed by Duncan's multiple-range test. Student's *t* test was used to detect significant differences between two groups. $p < 0.05$ was considered statistically significant.

ACKNOWLEDGMENTS

This work was supported by National Heart, Lung, and Blood Institute Grants HL057244, HL0765316, and HL091464.

REFERENCES

Allen JA, Halverson-Tamboli RA, Rasenick MM (2007). Lipid raft microdomains and neurotransmitter signalling. Nat Rev Neurosci 8, 128–140.

Baader AP, Buchler L, Bircher-Lehmann L, Kleber AG (2002). Real time, confocal imaging of Ca(2+) waves in arterially perfused rat hearts. Cardiovasc Res 53, 105–115.

Bao JX, Jin S, Zhang F, Wang ZC, Li N, Li PL (2010a). Activation of membrane NADPH oxidase associated with lysosome-targeted acid sphingomyelinase in coronary endothelial cells. Antioxid Redox Signal 12, 703–712.

Bao JX, Xia M, Poklis JL, Han WQ, Brimson C, Li PL (2010b). Triggering role of acid sphingomyelinase in endothelial lysosome-membrane fusion and dysfunction in coronary arteries. Am J Physiol Heart Circ Physiol 298, H992–H1002.

Belusa R, Wang ZM, Matsubara T, Sahlgren B, Dulubova I, Nairn AC, Ruoslahti E, Greengard P, Aperia A (1997). Mutation of the protein kinase C phosphorylation site on rat alpha1 Na+,K+-ATPase alters regulation of intracellular Na+ and pH and influences cell shape and adhesiveness. J Biol Chem 272, 20179–20184.

Bollinger CR, Teichgraber V, Gulbins E (2005). Ceramide-enriched membrane domains. Biochim Biophys Acta 1746, 284–294.

Brown DA (2006). Lipid rafts, detergent-resistant membranes, and raft targeting signals. Physiology (Bethesda) 21, 430–439.

Cherukuri A, Dykstra M, Pierce SK (2001). Floating the raft hypothesis: lipid rafts play a role in immune cell activation. Immunity 14, 657–660.

DeCoursey TE, Cherny VV, DeCoursey AG, Xu W, Thomas LL (2001). Interactions between NADPH oxidase-related proton and electron currents in human eosinophils. J Physiol 535, 767–781.

Fillet M, Van Heugen JC, Servais AC, De Graeve J, Crommen J (2002). Separation, identification and quantitation of ceramides in human cancer cells by liquid chromatography-electrospray ionization tandem mass spectrometry. J Chromatogr A 949, 225–233.

Forgac M (2007). Vacuolar ATPases: rotary proton pumps in physiology and pathophysiology. Nat Rev Mol Cell Biol 8, 917–929.

Gupta N, DeFranco AL (2003). Visualizing lipid raft dynamics and early signaling events during antigen receptor-mediated B-lymphocyte activation. Mol Biol Cell 14, 432–444.

Han WQ, Xia M, Zhang C, Zhang F, Xu M, Li NJ, Li PL (2011). SNARE-mediated rapid lysosome fusion in membrane raft clustering and dysfunction of bovine coronary arterial endothelium. Am J Physiol Heart Circ Physiol 301, H2028–H2037.

Henderson LM (1998). Role of histidines identified by mutagenesis in the NADPH oxidase-associated H +channel. J Biol Chem 273, 33216–33223.

Jefferies KC, Cipriano DJ, Forgac M (2008). Function, structure and regulation of the vacuolar (H+)-ATPases. Arch Biochem Biophys 476, 33–42.

Jimenez T, Sanchez G, Wertheimer E, Blanco G (2010). Activity of the Na, K-ATPase alpha4 isoform is important for membrane potential, intracellular Ca2+, and pH to maintain motility in rat spermatozoa. Reproduction 139, 835–845.

Jin S, Yi F, Zhang F, Poklis JL, Li PL (2008a). Lysosomal targeting and trafficking of acid sphingomyelinase to lipid raft platforms in coronary endothelial cells. Arterioscler Thromb Vasc Biol 28, 2056–2062.

Jin S, Zhang Y, Yi F, Li PL (2008b). Critical role of lipid raft redox signaling platforms in endostatin-induced coronary endothelial dysfunction. Arterioscler Thromb Vasc Biol 28, 485–490.

Kuebler WM, Yang Y, Samapati R, Uhlig S (2010). Vascular barrier regulation by PAF, ceramide, caveolae, and NO—an intricate signaling network with discrepant effects in the pulmonary and systemic vasculature. Cell Physiol Biochem 26, 29–40.

Lafourcade C, Sobo K, Kieffer-Jaquinod S, Garin J, van der Goot FG (2008). Regulation of the V-ATPase along the endocytic pathway occurs through reversible subunit association and membrane localization. PLoS One 3, e2758.

Lang PA, Graf D, Boini KM, Lang KS, Klingel K, Kandolf R, Lang F (2011). Cell volume, the serum and glucocorticoid inducible kinase 1 and the liver. Z Gastroenterol 49, 713–719.

Li PL, Zhang Y, Yi F (2007). Lipid raft redox signaling platforms in endothelial dysfunction. Antioxid Redox Signal 9, 1457–1470.

Li X, Becker KA, Zhang Y (2010). Ceramide in redox signaling and cardiovascular diseases. Cell Physiol Biochem 26, 41–48.

Li YP, Chen W, Liang Y, Li E, Stashenko P (1999). Atp6i-deficient mice exhibit severe osteopetrosis due to loss of osteoclast-mediated extracellular acidification. Nat Genet 23, 447–451.

Mantegazza AR, Savina A, Vermeulen M, Perez L, Geffner J, Hermine O, Rosenzweig SD, Faure F, Amigorena S (2008). NADPH oxidase controls phagosomal pH and antigen cross-presentation in human dendritic cells. Blood 112, 4712–4722.

Nieminen J, Kuno A, Hirabayashi J, Sato S (2007). Visualization of galectin-3 oligomerization on the surface of neutrophils and endothelial cells using fluorescence resonance energy transfer. J Biol Chem 282, 1374–1383.

Oehlke O, Martin HW, Osterberg N, Roussa E (2011). Rab11b and its effector Rip11 regulate the acidosis-induced traffic of V-ATPase in salivary ducts. J Cell Physiol 226, 638–651.

Perrotta C *et al.* (2010). Syntaxin 4 is required for acid sphingomyelinase activity and apoptotic function. J Biol Chem 285, 40240–40251.

Pike LJ (2006). Rafts defined: a report on the Keystone Symposium on Lipid Rafts and Cell Function. J Lipid Res 47, 1597–1598.

Reinehr R, Haussinger D (2007). Hyperosmotic activation of the CD95 system. Methods Enzymol 428, 145–160.

Schuchman EH (2010). Acid sphingomyelinase, cell membranes and human disease: lessons from Niemann-Pick disease. FEBS Lett 584, 1895–1900.

Schwarzer C, Machen TE, Illek B, Fischer H (2004). NADPH oxidase-dependent acid production in airway epithelial cells. J Biol Chem 279, 36454–36461.

Shao D, Segal AW, Dekker LV (2003). Lipid rafts determine efficiency of NADPH oxidase activation in neutrophils. FEBS Lett 550, 101–106.

Sun-Wada GH, Tabata H, Kawamura N, Aoyama M, Wada Y (2009). Direct recruitment of H+-ATPase from lysosomes for phagosomal acidification. J Cell Sci 122, 2504–2513.

Tabata H, Kawamura N, Sun-Wada GH, Wada Y (2008). Vacuolar-type H(+)-ATPase with the a3 isoform is the proton pump on premature melanosomes. Cell Tissue Res 332, 447–460.
Tojo A, Guzman NJ, Garg LC, Tisher CC, Madsen KM (1994). Nitric oxide inhibits bafilomycin-sensitive H(+)-ATPase activity in rat cortical collecting duct. Am J Physiol 267, F509–F515.
Van Munster EB, Kremers GJ, Adjobo-Hermans MJ, Gadella TW Jr (2005). Fluorescence resonance energy transfer (FRET) measurement by gradual acceptor photobleaching. J Microsc 218, 253–262.
Varsano S, Rashkovsky L, Shapiro H, Radnay J (1998). Cytokines modulate expression of cell-membrane complement inhibitory proteins in human lung cancer cell lines. Am J Respir Cell Mol Biol 19, 522–529.
Yamazaki S, Iwama A, Morita Y, Eto K, Ema H, Nakauchi H (2007). Cytokine signaling, lipid raft clustering, and HSC hibernation. Ann NY Acad Sci 1106, 54–63.
Yi F, Zhang AY, Janscha JL, Li PL, Zou AP (2004). Homocysteine activates NADH/NADPH oxidase through ceramide-stimulated Rac GTPase activity in rat mesangial cells. Kidney Int 66, 1977–1987.
Zhang AY, Yi F, Jin S, Xia M, Chen QZ, Gulbins E, Li PL (2007). Acid sphingomyelinase and its redox amplification in formation of lipid raft redox signaling platforms in endothelial cells. Antioxid Redox Signal 9, 817–828.
Zhang AY, Yi F, Zhang G, Gulbins E, Li PL (2006). Lipid raft clustering and redox signaling platform formation in coronary arterial endothelial cells. Hypertension 47, 74–80.
Zhang C, Li PL (2010). Membrane raft redox signalosomes in endothelial cells. Free Radic Res 44, 831–842.
Zou XP, Chen M, Zhang XQ, Zhang B, Cao J, Luo HS (2010). Expression of vacuolar H+-ATPases and the intracellular pH values in three adenocarcinoma cell lines of digestive system. Cell Mol Biol (Noisy-le-grand) 56 (suppl), OL1268–OL1275.